# Data-Driven Distributionally Robust Hierarchical Coordination for Home Energy Management

Hossein Saberi, Cuo Zhang, *Member, IEEE*, and Zhao Yang Dong, *Fellow, IEEE*

***Abstract*—Home energy management (HEM) is conventionally formulated using central control or local control methods assuming known accurate probability distributions of uncertainties. Without coordination between the central and the local control hierarchies, mutual impacts cannot be properly considered and addressed, which undermine operation efficiency of HEM. Moreover, the probability distributions always have errors, even in emerging data-based methods. To address these unsolved issues, firstly, this paper proposes a new hierarchical coordination method for HEM. On the central hierarchy, a central controller optimizes schedule of non-thermal loads to minimize daily operating cost. On the local hierarchy, automatic local controllers respond to real-time variations of their corresponding thermal zone temperatures to fulfill customer thermal comfort requirements. Secondly, using a finite training dataset, a data-driven distributionally robust optimization (DRO) method is proposed to guarantee solution robustness against worst probability distribution of multiple uncertainties. The hierarchical coordination method is formulated as a DRO model using the Wasserstein metric, which can be solved with high computing efficiency. Numerical simulations validate high solution robustness and overall optimum of the proposed method, fully addressing mutual impacts and uncertainties. Moreover, the proposed method could efficiently save the daily electricity bill by 11%, compared to conventional methods.**

***Index Terms*—Data driven optimization, distributionally robust optimization, flexible load, hierarchical coordination, home energy management, Wasserstein metric, uncertainty.**

## NOMENCLATURE

*Sets*

| | |
|---|---|
| $\Omega^l$ | All non-thermal controllable loads. |

*Indices*

| | |
|---|---|
| $\overline{\{.\}}/\underline{\{.\}}$ | Upper/lower limits of a variable |
| $\tilde{\{.\}}$ | Predicted value of an uncertain parameter |
| $\hat{\{.\}}$ | Realized value of a variable or an uncertain parameter |
| $l$ | Non-thermal controllable loads |
| $i$ | Training sample |
| $t$ | Discretized time for thermal loads model |
| $t'$ | Discretized time for DTSC strategy |
| $t''$ | Discretized time for non-thermal loads model. |

*Parameters*

| | |
|---|---|
| $\eta_{ev}$ | Charging efficiency of electric vehicle |
| $\eta_{sl}$ | Energy conversion efficiency of solar collector |
| $\overline{p}_g$ | Maximum deliverable power from distribution grid ($kW$) |
| $\rho$ | Constraint violation penalty factor ($\$/^oCh$) |
| $\tau/\tau''$ | Time step size for thermal/non-thermal loads ($h$) |
| $\tau'$ | Time step size for DTSC strategy ($h$) |
| $\xi$ | Vector of all uncertain parameters |
| $A_{sl}$ | Size of solar collector ($m^2$) |
| $A_{wt}$ | Heat loss effective area of water tank ($m^2$) |
| $A_w$ | Effective window of room ($m^2$) |
| $c$ | Electricity price ($\$/kWh$) |
| $C_r$ | Heat capacity of room ($kWh/^oC$) |
| $C_{wt}$ | Heat capacity of water tank ($kWh/^oC$) |
| $e$ | Prediction error |
| $E_d$ | Energy demand of electric vehicle ($kW$) |
| $E_\delta$ | Hourly energy limit ($kW$) |
| $H$ | Required operating time of non-interruptible loads ($h$) |
| $I$ | Forecasted solar irradiance ($kW/m^2$) |
| $L$ | A large number |
| $N$ | Number of samples inside training dataset |
| $p_{ncl}$ | Forecasted non-controllable power consumption ($kW$) |
| $p_{sl}$ | Heat from solar collector ($kW$) |
| $p_s$ | Water tank support for HVAC system ($kW$) |
| $p_{wd}$ | Forecasted hot water demand ($kW$) |
| $R_o$ | Equivalent thermal resistance of room envelopes ($^oC/kW$) |
| $T_o$ | Forecasted outdoor (ambient) temperature ($^oC$) |
| $U_{wt}$ | Heat loss coefficient of water tank due to radiation |
| $U_w$ | Room heat gain factor from solar irradiance. |

*Variables*

| | |
|---|---|
| $E$ | Energy state of electric vehicle ($kWh$) |
| $p_h$ | Energy produced/consumed by auxiliary heater ($kW$) |
| $p_u$ | Heat absorbed/produced by HVAC system ($kW$) |
| $T_r$ | Room temperature ($^oC$) |
| $T_{low}$ | Lower temperature set-point of HVAC controller ($^oC$) |

Manuscript received November 26, 2020; revised February 26, 2021; accepted June 4, 2021. Date of publication June 11, 2021; date of current version August 23, 2021. This work was supported in part by the ARC Research Hub for Integrated Energy Storage Solutions under Grant IH180100020, and in part by UNSW Digital Grid Futures Institute. Paper no. TSG-01766-2020. *(Corresponding author: Cuo Zhang.)*

The authors are with the School of Electrical Engineering and Telecommunications, The University of New South Wales, Sydney, NSW 2052, Australia (e-mail: h.saberi@unsw.edu.au; cuo.zhang@unsw.edu.au; zydong@ieee.org)

Color versions of one or more figures in this article are available at https://doi.org/10.1109/TSG.2021.3088433.

Digital Object Identifier 10.1109/TSG.2021.3088433

| | |
|---|---|
| $T_s$ | Temperature set-point of WH controller ($^oC$) |
| $T_{up}$ | Upper temperature set-point of HVAC controller ($^oC$) |
| $T_{wt}$ | Water tank temperature ($^oC$) |
| $u$ | Binary indicating on/off status of loads |
| $x$ | Vector of all decision variables. |

## I. Introduction

With emerging advance in smart metering and control technologies, energy management in residential and commercial buildings has attracted significant research interests. Optimal energy management in the buildings that contribute to more than 40% of global electricity consumption plays an important role in economic operation of power systems [1]. By coordinated operation of smart buildings, effective demand response programs could be implemented [2]. Moreover, while individual smart buildings as price-taker entities separately participate in passive demand response programs, by coordinated operation of multiple smart buildings, they can also participate as an aggregated price-maker entity in proactive demand response programs [3]. A smart building can be comprised of multiple thermal and electric components, such as solar thermal collectors, different types of energy storage systems (ESSs), and various controllable electric loads. Herein, the electric loads can be classified into thermal loads which convert electric energy to thermal one such as heating, ventilation, and air conditioning (HVAC) and water heating (WH) systems, and non-thermal loads such as washing machines and dryers. For the ESSs, since battery investment costs are still high [4], thermal ESSs such as hot water tanks, storing thermal energy from the collectors and WH systems, provide a good potential to improve overall building energy utilization efficiency [5], [6]. Thus, a highly efficient smart building is expected to employ solar thermal collectors, hot water tanks, and controllable thermal and non-thermal electric loads.

To minimize building energy usage cost, a home energy management (HEM) system which optimizes all the controllable components is required. Among these components, the thermal loads including HVAC systems consume near 50% of total electric energy [7], attracting research focuses on their models and control methods. In [8], detailed formulation for integrated control of HVAC system, lighting, and shading is proposed, capturing thermal interaction between different components of building. In [9], a real-time thermal energy management system for engaging smart buildings in demand response programs is proposed. In [10], relying on an autonomous cycle of data analysis tasks, a self-managing structure for multi-HVAC systems is proposed. However, these works focus on management of thermal loads without consideration of non-thermal loads, such that overall operation efficiency is restricted. In [11], a multi-objective approach in mixed integer non-liner programming (MINLP) is proposed to optimize the user convenience rate and thermal comfort along with the energy bill. In [12], optimal operation of different household appliances with focus on capturing thermal load uncertainties is studied through a mixed integer linear programming (MILP) model. In [13], a smart building is considered as a grid-tied microgrid where a master-slave control scheme is introduced for coordination of different power sources. The study in [14] presents a novel HEM system for coordination of multiple thermal and non-thermal loads considering lifestyle-related operational dependency of household appliances. [15] proposes a MILP model for integration of electric vehicles (EVs), ESSs, and renewable power generation in a HEM problem. In [16], an integrated HEM system based on Markovian process is proposed to minimize the consumer daily bill while considering different operational constraints in an probabilistic manner. However, these research works are central scheduling approaches that cannot effectively address real-time variations of uncertain parameters such as solar irradiance, ambient temperature and thermal demand.

To this end, [17] develops a local control method to adjust day-ahead scheduling decisions based on real-time data. However, such a local control cannot guarantee the optimum HEM over the whole day operation horizon. Other works [18], [19] consider thermostatically controlled loads, which are in fact a local control method without optimizing set-points of local controllers. In fact, in these methods, by estimating the amount of thermal loads, the estimated impact of the local control is projected in the central control models, but the dynamic real-time impact is not considered. Furthermore, the central controller has no control over the local controller. This means only the estimated impact of local control on central control is considered, but not the impact of central control on local control. Thus, the mutual impacts are not considered and addressed. Considering their respective advantages and limitations, it is sensible to hierarchically coordinate the central control methods and the local ones. Besides, in practice, thermal loads are locally triggered to be on/off by conditions if temperature crosses a preset set-points which are imperative to be optimized to acquire maximum efficiency. In this way, mutual impacts between the central and the local control are expected to be fully considered and addressed in the optimization.

In addition, it is worth noting that different thermal and electric components have different responding speeds. Scheduling of non-thermal loads is mainly affected by electricity prices, such that washing machines and dryers should be scheduled in a relatively long timescale, e.g., half an hour, to meet the price update interval. On the contrary, a small timescale, e.g., 5 minutes, is required to accurately model thermodynamics associated to thermal loads. Thus, multiple components should be modeled considering their respective responding characteristics. However, since the above works [6], [14] consider only one specified timescale, the multiple components cannot be efficiently coordinated.

In terms of dealing with uncertainty, conventional works use deterministic formulation relying on predictions of uncertainty [14], [15], but solution efficiency is significantly impaired by prediction errors. To address the prediction errors, deterministic approaches are executed through a rolling horizon method with smaller prediction intervals [19], [20]. However, uncertainties are still considerable for a normal planning horizon of one day. To more efficiently address uncertainties, advanced optimization techniques such as stochastic

optimization (SO) [6] and robust optimization (RO) [21] are developed and applied for power system problems. SO methods assume that accurate probability distribution functions (PDFs) of prediction errors are well known. However, in practice, limited historical data leads to inaccurate PDFs and thereby inefficient uncertainty modeling. Besides, it is computationally expensive for SO methods, due to including a large number of scenarios to present probability distributions. With no requirement of uncertainty probability information, RO methods can obtain robust solutions under only the worst case of uncertainty realization, achieving high computing efficiency. However, the RO solutions can be too conservative, since the worst case could be of considerably low probability.

With advanced metering technologies, smart buildings are capable for data collecting and processing. This new smart environment can assist various artificial intelligence based techniques by providing training datasets for parameter estimation [22] and data-driven building models can be formulated. However, regarding optimization, RO and SO methods cannot properly take advantages of available datasets. As such, SO methods still suffer from presumption of an accurate PDF and RO methods can only update boundaries of uncertain parameters without efficient use of datasets. Therefore, it is sensible to develop data-driven optimization methods that suit the advanced data-based smart environment.

To tackle disadvantages of both SO and RO techniques, data-driven distributionally robust optimization (DRO) methods are developed. Using a finite historical training dataset, data-driven DRO methods obtain the minimal expected value of objective over the worst probability distribution belonging to an ambiguity set of all possible distributions. Based on definition of ambiguity set, data-driven DRO methods can be classified into moment-based [23] and statistical-distance-based methods such as Kullback-Leibler divergence [24] or Wasserstein metric [25]. Recently, the moment-based DRO method has been applied in HEM problems [26], [27] with a basic assumption that moments of true probability distribution of uncertainty parameters such as mean and covariance are already known based on the finite available data. However, this assumption is not necessarily correct in practice. Moreover, it is shown that the worst probability distribution obtained by the moment-based methods could lead to remarkably conservative solutions [28], [29]. On the other hand, considering all distributions that are close, in terms of statistical distances such as Wasserstein distance, to a nominal distribution, the statistical-distance-based methods can be a more efficient alternative. The statistical-distance-based methods have been applied in power system studies such as optimal power flow [30] and unit commitment [31]. For HEM research, moment-based DRO chance-constrained formulation is developed by [26] to address prediction errors, but HVAC systems and associated thermodynamics are not considered. Similarly, the work in [27] considers ambient temperature prediction errors only, while non-thermal loads and other sources of uncertainty are not modeled. Thus, there is a gap for developing comprehensive models that tackle various sources of uncertainty, specially by employing data-driven statistical-distance-based DRO methods.

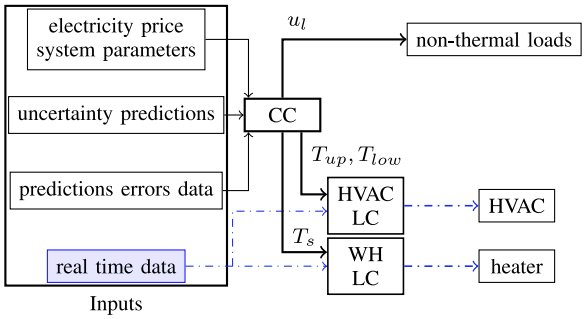


Fig. 1. The proposed hierarchical coordination structure.

In literature, hierarchical coordination has not been developed for HEM and uncertainties have not been efficiently tackled. To this point, firstly, this paper proposes a new hierarchical coordination method which coordinates a central controller (CC) and two automatic local controllers (LCs), to minimize weighted summation of daily operating cost and conditional value at risk (CVaR) of operating constraint violations. The CC determines optimal schedule of day-ahead non-thermal loads as well as set-points of LCs. In addition, new linear constraints are proposed to model the LCs associated to HVAC and WH systems. Secondly, a data-driven statistical-distance-based DRO method is proposed to solve the hierarchical coordination problem. With finite historical datasets, this paper utilizes Wasserstein metric to define ambiguity sets including all PDFs within a probability distance of Wasserstein radius, to deal with multiple uncertainties of solar irradiance, solar production, ambient temperature and hot water demand. Moreover, it provides decision makers with flexibility to adjust solution robustness by modifying the Wasserstein radius. In addition to having superior out-of-sample performance, the proposed DRO method is computationally tractable. Thus, this paper proposes a data-driven distributionally robust hierarchical coordination method for HEM.

The major contributions of this paper are summarized as follows.

- A hierarchical coordination method for HEM to simultaneously optimize central and local controllers, thoroughly considering their mutual impacts.
- Efficient linear constraints which model automatic local controllers to allow optimizing set-points of local controllers in a HEM optimization problem.
- A data-driven DRO method for the HEM problem with Wasserstein metric to provide robust solutions and superior out-of-sample performance under uncertainties.

## II. Hierarchical Coordination Method

This paper proposes a hierarchical coordination method which can fully get benefit of central and local control and address the mutual impacts. This method contains two control hierarchies, i.e., a CC on the higher hierarchy and two automatic LCs for the HVAC and WH systems, respectively on the lower one. The structure of this hierarchical coordination is illustrated in Fig. 1.

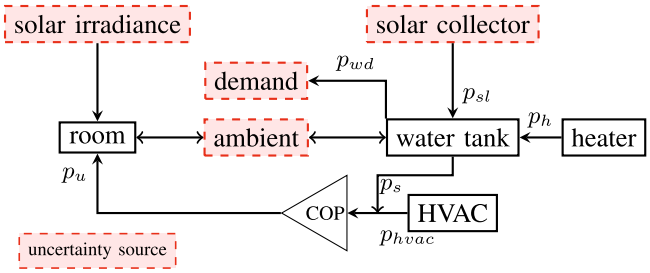


Fig. 2. The thermal loads elements.

The input data for CC are day-ahead electricity price profile, system parameters, prediction of uncertainties, and historical records of prediction errors. The CC receives the input data and executes the HEM optimization program to determine the on-off schedule of different non-thermal loads, i.e., $u_l$, the set-points of the HVAC LC, i.e., $T_{up}, T_{low}$, and the set-point of the WH LC, i.e., $T_s$.

On the other hand, a dynamic temperature set-point control (DTSC) strategy is utilized to provide the LCs with more flexibility. In this strategy, the LC set-points are dynamically updated to a predefined value which is determined by CC at beginning of each DTSC time interval. In this paper, DTSC interval is $t' = 15min$. During the DTSC, LCs receive and automatically respond to real-time variations of their relevant thermal zone temperatures by turning on/off the HVAC and/or WH thermal energy generation units. As discussed in Section III-E in this paper, the LC logic is linearly modeled and included in the HEM optimization program such that the higher-level CC and lower-level LCs are hierarchically coordinated to achieve optimal operation over 24-hour operation horizon.

## III. System Model

This paper considers a smart home system including three non-thermal loads with different characteristics in terms of deferrability and interruptibility, a hybrid solar assisted HVAC-WH system, and two thermal zones, i.e., one water tank and one room. Fig. 2 illustrates the thermal loads and the thermal interactions among them. In this figure, the uncertainty sources are indicated by colored boxes.

The following subsections describe the proposed model for different elements of this smart home system.

### A. Thermal Zone Models

Thermal zone models follow the first law of thermodynamics, i.e., heat balance, that in a closed form can be formulated by the following differential equation,

$$C\frac{dT}{dt} = Q,$$

where $C$ is heat capacity, $T$ is zone temperature, and $Q$ is net heat change rate. This differential equation can be further described by a discretized form as,

$$C\left(T^{t+\tau} - T^{t}\right) = \tau Q^{t},$$

provided that the discretization time step $\tau$ is small enough with consideration of the large heat capacity.

As illustrated in Fig. 2, the water tank zone exchanges heat with ambient environment, supports hot water demand and the HVAC system condenser, and receives thermal energy from the solar collector and/or an auxiliary electrical heater. As such, the thermal dynamics of the hot water tank is modeled as follows.

$$T_{wt}^{t+\tau,i} = \left(1 - \frac{\tau U_{wt}A_{wt}}{C_{wt}}\right)T_{wt}^{t,i} + \frac{\tau U_{wt}A_{wt}}{C_{wt}}T_{o}^{t,i} + \frac{\tau}{C_{wt}}\left(p_{h}^{t,i} + p_{sl}^{t,i} - p_{wd}^{t,i} - p_{s}^{t,i}\right) \quad (1)$$

The room zone exchanges heat with ambient environment, receives heat from solar irradiance and cooling/heating from the HVAC system. The thermal dynamics of the room is modeled as follows.

$$T_{r}^{t+\tau,i} = \left(1 - \frac{\tau}{R_o C_r}\right)T_{r}^{t,i} + \frac{\tau}{R_o C_r}T_{o}^{t,i} + \frac{\tau U_w A_w}{C_r}I^{t,i} + \frac{\tau p_u^{t,i}}{C_r} \quad (2)$$

Thermal zone temperatures are required to be maintained in a desired range as formulated by (3) and (4).

$$\underline{T}_{wt} \le T_{wt}^{t,i} \le \overline{T}_{wt} \quad (3)$$

$$\underline{T}_{r}^{t} \le T_{r}^{t,i} \le \overline{T}_{r}^{t}. \quad (4)$$

### B. Hybrid HVAC-WH System Model

The HVAC system comprises of different elements such as pumps and fans, cooling tower, cooling and heating coils, etc. Despite the different types of HVAC system elements, the HVAC system is modeled with its coefficient of performance (COP) that is calculated through dividing an amount of produced heating/cooling by consumed electric energy. It is indicated by [5] that COP of HVAC systems with chillers of vapor absorption type can considerably be improved in combination with hot water tanks. In this configuration, the hot water tank supports thermal demand of the HVAC system condenser, with an amount of $p_s$, increasing the overall COP as follows [6]. $p_u = COP_a(p_{hvac} + p_s) = COP_c p_{hvac}$. By knowing COPs of the system in standalone (a) and combined (c) modes for cooling ($-$) and heating ($+$) applications, the absorbed/produced heat by HVAC system is modeled by (5).

$$p_u^{t,i} = COP_a^{+} p_{hvac}^{a,+,t,i} + COP_c^{+} p_{hvac}^{c,+,t,i} - COP_a^{-} p_{hvac}^{a,-,t,i} - COP_c^{-} p_{hvac}^{c,-,t,i} \quad (5)$$

The heat energy from the hot water tank is calculated by (6).

$$p_s^{t,i} = \frac{COP_c^{+} - COP_a^{+}}{COP_a^{+}} p_{hvac}^{c,+,t,i} + \frac{COP_c^{-} - COP_a^{-}}{COP_a^{-}} p_{hvac}^{c,-,t,i} \quad (6)$$

During each time interval, only one mode can be selected, which is constrained as follows.

$$u_{hvac}^{a,+,t,i} + u_{hvac}^{c,+,t,i} + u_{hvac}^{a,-,t,i} + u_{hvac}^{c,-,t,i} \le 1 \quad (7)$$

In practice, HVAC systems operate at certain rated power as imposed by (8)-(11). For the sake of simplicity, this paper uses

one rated operation point as below. However, multiple rated operation points can be modeled similarly.

$$p_{hvac}^{a,+,t,i} = p_{hvac}^{rated} u_{hvac}^{a,+,t,i} \tag{8}$$

$$p_{hvac}^{c,+,t,i} = p_{hvac}^{rated} u_{hvac}^{c,+,t,i} \tag{9}$$

$$p_{hvac}^{a,-,t,i} = p_{hvac}^{rated} u_{hvac}^{a,-,t,i} \tag{10}$$

$$p_{hvac}^{c,-,t,i} = p_{hvac}^{rated} u_{hvac}^{c,-,t,i} \tag{11}$$

The HVAC system power consumption is computed by (12).

$$p_{hvac}^{t,i} = p_{hvac}^{a,+,t,i} + p_{hvac}^{c,+,t,i} + p_{hvac}^{a,-,t,i} + p_{hvac}^{c,-,t,i} \tag{12}$$

Moreover, the solar collector generates thermal power depending on its size, efficiency, and solar irradiance as $p_{sl}^{t} = \eta_{sl} I^{t} A_{sl}$. Regarding the nature of varying energy conversion efficiency $\eta_{sl}$, solar collector power generation is considered as an independent uncertainty parameter.

Power usage of the auxiliary heater is computed by (13).

$$p_{h}^{t,i} = p_{h}^{rated} u_{h}^{t,i}. \tag{13}$$

### C. Non-Thermal Load Models

The proposed hierarchical coordination method utilizes non-thermal controllable loads to save customer bills by using low-price electric energy. This papers considers three typical non-thermal controllable loads. It is worth noting that other non-thermal controllable loads can also be applied without affecting effectiveness of the proposed method, when necessary. Power consumption of all loads follows discrete states. For simplicity, this paper considers two states of on/off as below, but multiple states can be modeled similarly.

$$p_{l}^{t''} = u_{l}^{t''} p_{l}^{rated} \tag{14}$$

The loads are required to operate in specific time windows $[\alpha_l, \beta_l]$ as follows.

$$u_{l}^{t''} = 0, t'' \notin [\alpha_l, \beta_l]. \tag{15}$$

*1) Interruptible Deferrable Loads:* Here, EV is modeled as an interruptible deferrable load as follows [6]. The charging state of the EV $E_l$ in each time $t + \tau''$ is a function of the previous charging state, charging efficiency $\eta_{ev}$, and charging power $p_l$ as below.

$$E_{l}^{t''+\tau''} = E_{l}^{t''} + \eta_{ev} p_{l}^{t''} \tau'' \tag{16}$$

At the end of time window, the EV must be charged with sufficient energy higher than a predefined limit.

$$E_{l}^{\beta_l} \geq E_d \tag{17}$$

In addition, the energy limits of EV are imposed as follows.

$$\underline{E}_l \leq E_{l}^{t''} \leq \overline{E}_l. \tag{18}$$

*2) Non-Interruptible Deferrable Loads:* Non-interruptible deferrable loads with required operating time $H_l$ are modeled as follows.

$$\sum_{a=t''}^{t''+H_l-\tau''} u_{l}^{a} \geq \frac{H_l}{\tau''} \left( u_{l}^{t''} - u_{l}^{t''-\tau''} \right), t'' \in [\alpha_l, \beta_l] \tag{19}$$

In this paper, a washing machine is considered as a non-interruptible and deferrable load.

*3) Non-Interruptible Non-Deferrable Loads:* Non-interruptible non-deferrable loads are modeled as follows.

$$\sum_{t''=\alpha_l}^{\alpha_l+H_l-\tau''} u_{l}^{t''} \geq \frac{H_l}{\tau''} \tag{20}$$

In this paper, clothes dryer is considered as a non-interruptible non-deferrable load.

The total electric energy consumption is calculated by (21).

$$p_{total}^{t,i} = p_{hvac}^{t,i} + p_{h}^{t,i} + \sum_{l \in \Omega^l} p_{l}^{t} \tag{21}$$

It is worth noting that based on the user preferences or specific logic of appliances, some loads need to be scheduled in a consecutive order. In this paper, this requirement is satisfied by setting the scheduling time intervals of appliances in a consecutive order. The proposed data-driven distributionally robust method can also adapt other models such as the logic based constraints [14], [32].

### D. System Constraints

The total power consumption by controllable loads at each time is limited by maximum available power by the power system $\overline{p}_g$ with consideration of power consumption of non-controllable loads $p_{ncl}$ as follows.

$$\sum_{l \in \Omega^l} p_{l}^{t''} + p_{hvac}^{t,i} + p_{h}^{t,i} \leq \overline{p}_g - p_{ncl}^{t} \quad \forall\, t, t'' | t'' \leq t < t'' + \tau'' \tag{22}$$

In addition to the power limits, the hourly energy consumption might be limited by the utility as follows.

$$\sum_{l \in \Omega^l} \sum_{a=\delta-1}^{\delta-\tau''} p_{l}^{a} \tau'' + \sum_{a=\delta-1}^{\delta-\tau} \left( p_{hvac}^{a,i} + p_{h}^{a,i} + p_{ncl}^{a} \right) \tau \leq E_\delta \quad \forall\, \delta \in \{1, 2, \ldots, 24\}. \tag{23}$$

### E. Local Controller Models

LCs are employed to respond to real-time variations of thermal zone temperature which are affected by the multiple uncertainties. The LC of the HVAC system activates the cooling mode when room temperature exceeds the upper set-point $T_{up}$ as follows.

$$\frac{T_{r}^{t,i} - T_{up}^{t'}}{L} \leq u_{hvac}^{a,-,t,i} + u_{hvac}^{c,-,t,i} \leq 1 + \frac{T_{r}^{t,i} - T_{up}^{t'}}{L}, \quad t \in \left[ t', t' + \tau' \right) \tag{24}$$

Similarly, it activates the heating mode when room temperature drops below the lower set-point $T_{low}$ as follows.

$$\frac{T_{low}^{t'} - T_{r}^{t,i}}{L} \leq u_{hvac}^{a,+,t,i} + u_{hvac}^{c,+,t,i} \leq 1 + \frac{T_{low}^{t'} - T_{r}^{t,i}}{L}, \quad t \in \left[ t', t' + \tau' \right) \tag{25}$$

Otherwise, the LC turns off the HVAC system.

The LC of the WH system turns on the electric heater when the water tank temperature drops below its set-point $T_s$.

Otherwise, it turns off the electric heater. The LC of the WH system is modeled as follows.

$$\frac{T_s^{t'} - T_{wt}^{t,i}}{L} \le u_h^{t,i} \le 1 + \frac{T_s^{t'} - T_{wt}^{t,i}}{L}, t \in \left[t', t' + \tau'\right) \quad (26)$$

It is noted that the LCs are dedicated to the thermal loads only. The schedule of the non-thermal loads is mainly affected by the energy price which is known in the prior day. Thus, the non-thermal loads are scheduled in the day-ahead scheduling model without local control.

### *F. Central Controller Objective*

In this paper, the proposed objective function aims to minimize weighted summation of the daily electricity usage bill and the CVaR of operating constraint violations. To this end, it is noted that the thermal zone constraints (1) and (2) can be reformulated by (27)-(28) and (29)-(30), respectively. Herein, $x$ is the vector of all variables, $\xi$ is the vector of all uncertain parameters as given by (31) and $g_{wt}$ and $g_r$ express linear functions.

$$g_{wt}\left(x^{t,i}, \xi^{t,i}\right) \le 0 \quad (27)$$

$$-g_{wt}\left(x^{t,i}, \xi^{t,i}\right) \le 0 \quad (28)$$

$$g_r\left(x^{t,i}, \xi^{t,i}\right) \le 0 \quad (29)$$

$$-g_r\left(x^{t,i}, \xi^{t,i}\right) \le 0 \quad (30)$$

$$\xi^t = \left[T_o^t, I^t, p_{wd}^t, p_{sl}^t\right] \quad (31)$$

According to [33], the $\zeta$-CVaR, i.e., CVaR with a risk level $\zeta$, of each constraint violation in (27)-(30) can be formulated by a point-wise maximum function. For example, the following function corresponds to (27).

$$\ell_1^t = \max_{\theta_1^t}\left\{\left(g_{wt}\left(x^{t,i}, \xi^{t,i}\right) - \theta_1^t\right)/(1-\zeta) + \theta_1^t, \theta_1^t\right\} \ \forall i. \quad (32)$$

Here, the argmin of (32), i.e., $\hat{\theta}_1^t$, is the $\zeta$-CVaR of the constraint violation in (27). As such, there are four point-wise maximum functions corresponding to the $\zeta$-CVaR of (27)-(30) that can be reformulated as follows.

$$\ell_j^t = \max_{\theta^t}\left\{b_{kj}^t\left(x^{t,i}, \theta^t\right) + \left\langle a_{kj}^t\left(x^{t,i}, \theta^t\right), \xi^{t,i}\right\rangle\right\}, \quad \forall i, k = 1, 2, j = 1, 2, 3, 4 \quad (33)$$

It is noted that since the major focus of the proposed hierarchical coordination method is to address the thermal constraint violations, in this paper, only the uncertainty of parameters affecting the thermal constraints is taken into account. In general, other sources of uncertainty such as non-controllable loads can also be considered in the proposed data-driven DRO-based model through a similar approach. In a SO form, the proposed objective function minimizing the expected value of the weighted summation is formulated as follows.

$$\mathcal{L}(x, \xi) = \min_{x,\theta}\left\{\sum_{t=0}^{24}\left\{\rho \sum_{j=1}^{4} \ell_j^t\left(x^t, \xi^t\right) + \frac{1}{N}\sum_{i=1}^{N} \tau c^t p_{total}^{t,i}\right\}\right\} \quad (34)$$

It is noted that $\ell_j^t(x^t, \xi^t)$ is a maximization problem itself. However, (34) is not further simplified here as this objective function will be reformulated and extended to a general DRO-based formulation in the next section.

## IV. Data-Driven Distributionally Robust Optimization

The proposed hierarchical coordination method considers uncertainties such as solar irradiance $I^t$, solar production $p_{sl}^t$, ambient temperature $T_o^t$ and hot water demand $p_{wd}^t$. To address these uncertainties, this paper proposes a data-driven DRO method optimizing HEM problem with a finite historical training dataset. In this method, the worst PDF of uncertainty is searched within an ambiguity set consisting of all possible PDFs built on the dataset, and the problem is solved under this worst PDF. Thus, a robust solution against all the PDFs is expected.

### *A. Uncertainty Model*

As shown in Fig. 2, the thermal loads are affected by various sources of uncertainty such as solar irradiance, solar collector production, hot water demand, and ambient temperature. These uncertainty parameters are modeled as summation of predicted values and prediction errors as follows.

$$I^{t,i} = \tilde{I}^t + e_I^{t,i} \quad (35)$$

$$p_{sl}^{t,i} = \tilde{p}_{sl}^t + e_{p_{sl}}^{t,i} \quad (36)$$

$$p_{wd}^{t,i} = \tilde{p}_{wd}^t + e_{p_{wd}}^{t,i} \quad (37)$$

$$T_o^{t,i} = \tilde{T}_o^t + e_{T_o}^{t,i} \quad (38)$$

It is noted that in (35)-(38), the prediction errors are extracted from the finite historical training dataset without any assumption of uncertainty PDFs. The predicted values are obtained either from weather prediction agencies or separate prediction modules. These predicted values are then used in the proposed model as inputs.

### *B. Wasserstein Metric*

This paper applies Wasserstein metric to estimate difference between the true unknown distribution of uncertain parameters and the empirical distribution built on the finite training samples. The Wasserstein metric can minimize the expected value of a loss function with form (39) over the worst distribution $Q \in \mathcal{P}$, as formulated in (40).

$$\ell(x, \xi) = \max_k \{b_k(x) + \langle a_k(x), \xi\rangle\} \quad (39)$$

$$\inf_{x \in X} \sup_{Q \in \mathcal{P}} E^Q[\ell(x, \xi)] \quad (40)$$

Here, $x$ and $\xi$ denote vectors of decision variables and uncertainty parameters, respectively. $\langle a_k(x), \xi\rangle$ denotes the inner product of vectors $a_k(x)$ and $\xi$. $\mathcal{P}$ denotes the ambiguity set including all PDFs $Q$ that are within a probability distance, i.e., Wasserstein ball radius, of $\epsilon$ from $\hat{P}_N$. $\hat{P}_N$ is a discrete empirical PDF built on the prediction error samples, i.e., training dataset $\hat{\Xi}_N$, as given by (41).

$$\hat{P}_N = \frac{1}{N}\sum_{i=1}^{N} \delta_{\hat{\xi}_i} \quad (41)$$

The Wasserstein metric is defined on the probability space $\mathcal{M}(\Xi)$ including all PDFs $Q$ supported on uncertainty set $\Xi$ with the following.

$$E^Q[\|\xi\|] = \int_{\Xi} \|\xi\| Q(d\xi) < \infty$$

Here, Wasserstein distance $d_W$ between two PDFs $Q_1, Q_2 \in \mathcal{M}(\Xi)$ is defined by (42), wherein, $\Pi$ is the joint PDF of $\xi_1$ and $\xi_2$ with marginals $Q_1$ and $Q_2$, respectively .

$$d_W(Q_1, Q_2) = \inf \int_{\Xi^2} \|\xi_1 - \xi_2\| \Pi(d\xi_1, d\xi_2). \tag{42}$$

### C. DRO-Based HEM Model

With employing the Wasserstein metric, this paper finally proposes a DRO-based HEM model as follows.

$$\hat{O}_N = \min_{\substack{x,s,\theta,\\ \lambda\geq 0,\gamma}} \left\{ \sum_{t=0}^{24} \left\{ \sum_{j=1}^{4} \epsilon \lambda_j^t + \frac{1}{N} \sum_{i=1}^{N} \left( s_o^{t,i} + \sum_{j=1}^{4} s_j^{t,i} \right) \right\} \right\} \tag{43}$$

subject to:

$$\tau c^t p_{total}^{t,i} \leq s_o^{t,i} \quad \forall t, i \tag{44}$$

$$\rho\left(b_{kj}^t + \langle a_{kj}^t, \xi^{t,i} \rangle\right) + \langle d^t - \mathcal{C}^t \xi^{t,i}, \gamma_{kj}^{t,i} \rangle \leq s_j^{t,i}, \ \forall t, i, j, k \tag{45}$$

$$\left\| \mathcal{C}^{t\,\mathbf{T}} \gamma_{kj}^{t,i} - \rho a_{kj}^t \right\|_\infty \leq \lambda_j^t \quad \forall t, i, j, k \tag{46}$$

$$\gamma_{kj}^{t,i} \geq 0 \quad \forall t, i, j, k \tag{47}$$

$$(3)-(26) \tag{48}$$

Herein, $s_o$ defines the electric energy consumption cost, $\gamma$ is the vector of non-negative dual variables, as (47), related to the uncertainty set $\Xi$ which is a polytope defined by (49).

$$\Xi = \left\{ \xi^t \in R^m : \mathcal{C}^t \xi^t \leq d^t \right\} \tag{49}$$

$\mathcal{C}^{t\,\mathbf{T}}$ is transpose of the matrix $\mathcal{C}^t$. It is noted that objective (43) consists of three terms. The first term is ambiguity cost formed by product of the Wasserstein ball radius $\epsilon$ and the ambiguity penalty variable $\lambda$. The second term is the electricity consumption cost defined by (44). The third term is the CVaR of constraint violations as (45). In (46), the infinity norm is utilized to linearly define the ambiguity penalty variable $\lambda$. The Wasserstein ball radius $\epsilon$ can be used as a means for adjusting the level of solution robustness. Using a small $\epsilon$, the ambiguity set is closer to the empirical PDF (41) such that in the ambiguity-free case $\epsilon = 0$, the problem (43) becomes a conventional sample-average-approximation stochastic problem. On the contrary, a larger radius $\epsilon$ increases solution robustness.

By solving (43) under the training set $\hat{\Xi}_N$ with minimizers $\hat{x}_N$, the out-of-sample performance guarantee holds to fulfill the following chance constraint.

$$P_N\left\{ E^P\left[\mathcal{L}(\hat{x}_N, \xi)\right] \leq \hat{O}_N \right\} \geq 1 - \beta \tag{50}$$

Here, $\mathcal{L}(x, \xi)$ is the SO form of the total day-ahead objective cost as formulated by (34) which is equal to the ambiguity-free case $\epsilon = 0$ of (43). In other words, out-of-sample performance analysis states that if the obtained decisions $\hat{x}_N$ are taken, the expected cost of problem with new uncertainty samples $\xi$ is bounded by $\hat{O}_N$ with confidence level of $1 - \beta$. The proposed model (43) is a MILP problem which scales polynomially and thus can be efficiently solved by commercial solvers.

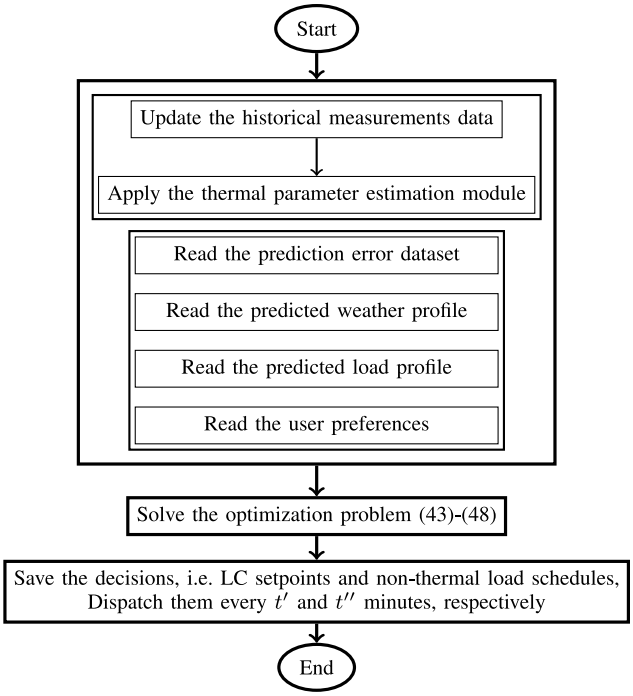


Fig. 3. Procedure of the proposed HEM method.

### D. Application Procedure

Fig. 3 illustrates the required steps for practical application of the proposed HEM method.

Prior to solving the optimization problem (43)-(48), several input parameters must be prepared. These inputs are categorized in two parts. The first part updates the historical measurement data by involving the previous-day measurements, and applies a thermal parameter estimation module to calculate the building thermal parameters. The second part reads the updated prediction error dataset, predicted weather and load profiles, and user thermal and non-thermal load preferences.

After solving the proposed DRO-based HEM problem, the decisions including the set-points of LCs and the schedule of non-thermal loads for the entire day are saved. The CC then dispatches these decisions to the LCs and the non-thermal loads for each period of $t'$ and $t''$ minutes, respectively.

## V. Numerical Analysis

### A. System Description

The proposed hierarchical coordination method is tested with parameters of a typical smart home. The room and hot water tank thermal parameters are given in Table I. The non-thermal controllable loads are described by Table II.

The energy conversion efficiency of solar collector is $\eta_{sl} = 0.5$. The COP of the hybrid HVAC-WH system in combined and stand alone modes is 5 and 3, respectively [6]. The predictions of solar irradiance and ambient temperature are

TABLE I
THE ROOM AND HOT WATER TANK THERMAL PARAMETERS

| $C_r$ $(kWh/^oC)$ | $R_o$ $(^oC/kW)$ | $A_w$ $(m^2)$ | $C_{wt}$ $(kWh/^oC)$ | $A_{wt}$ $(m^2)$ | $U_{wt}$ |
|---|---|---|---|---|---|
| 5.915 | 29.38 | 3.549 | 1.078 | 8.29 | 0.001 |

TABLE II
THE NON-THERMAL CONTROLLABLE LOADS PARAMETERS

| Load | EV | Washing machine | Clothes dryer |
|---|---|---|---|
| Type | 1 | 2 | 3 |
| Power | 3.3 kW | 0.5 kW | 2.5 kW |
| Time window | [17:00, 08:00] | [11:30, 17:00] | [17:00, 18:00] |
| Operation length | N/A | 2.5 hour | 1 hour |

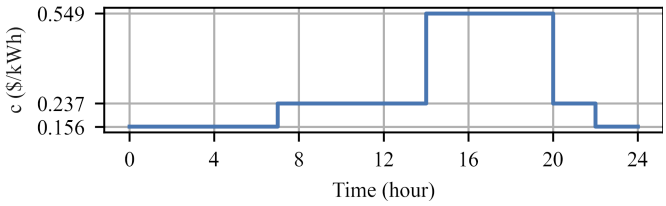


Fig. 4. The day-ahead electricity price profile.

extracted from [34] while the day-ahead electricity prices for a summer day in Sydney are shown in Fig. 4 [35]. The data of hot water demand prediction, total power limit, energy limit, solar collector and auxiliary heater in [6] are applied. The hot water tank and room temperatures are required in ranges of $[40^oC, 70^oC]$ and $[19^oC, 21^oC]$, respectively. Fig. 5 shows 20 prediction samples of ambient temperature, solar irradiance and hot water demand, where black curve indicates real measurement, i.e., $e^{t,i} = 0$. The prediction errors follow an increasing trend such that predictions are highly accurate at the beginning of scheduling horizon and the errors become large at the end. In this paper, prediction errors of ambient temperature, solar irradiance and hot water demand are generated by a sequential Monte Carlo simulation technique using a normal distribution function with a standard deviation of $0.015^oC/min$, $1.5W/min$, $0.75W/min$, respectively. In the sequential sample generation, the mean value of first time step is equal to zero, and the mean value of following time steps is equal to the prior time step sample. Without loss of generality, it is assumed that energy conversion efficiency of the solar collector is constant such that solar productions samples are proportional to the solar irradiance samples.

The DTSC strategy and non-thermal loads are modeled with time intervals of $\tau' = 15min$ and $\tau'' = 30min$, respectively. The differential equations related to thermal loads require small time intervals to accurately model the thermodynamics of thermal zones. However, it is noted that if the time interval is chosen too small, the size of program can grow significantly, bringing computational issues. In literature, different time intervals of $\tau = 30min$ [21], $\tau = 15min$ [15], [19], $\tau = 10min$ [9], [14] are widely used for thermal loads. In this paper, for the thermal loads, a small time interval of $\tau = 5min$

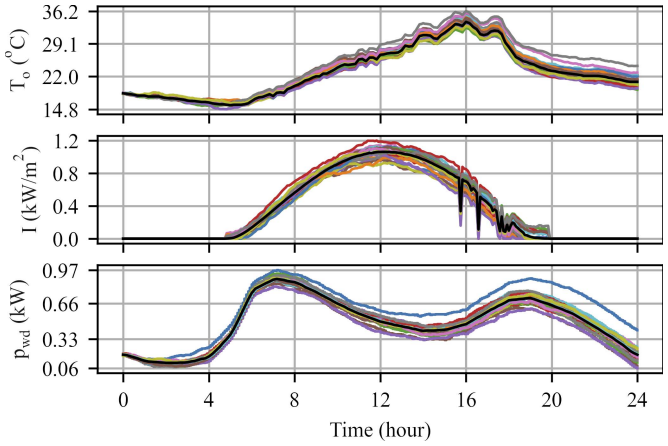


Fig. 5. The predictions of ambient temperature, solar irradiance and hot water demand.

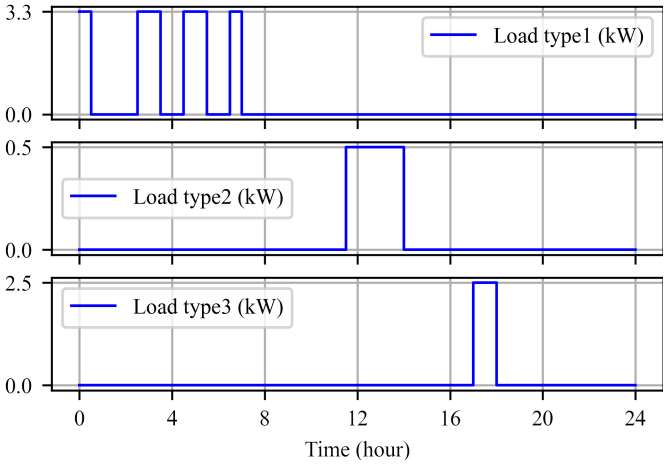


Fig. 6. Optimal schedule of the non-thermal loads.

is set to achieve an accurate model. The proposed DRO-based model is solved with a Wasserstein radius of $\epsilon = 0.001$ and a constraint violation penalty factor of $\rho = 24(\$/^oCh)$.

The optimization program is coded in Python and solved by GUROBI [36]. The simulations are conducted on a PC running at 3.2GHz with 16GB RAM.

### *B. Central Controller Decisions*

The CC solves the HEM problem (43) to obtain a robustly optimal day-ahead schedule. The 24-hour on/off schedule decisions of non-thermal loads and local controllers set-points are shown in Fig. 6 and Fig. 7, respectively.

As seen in Fig. 6, the load type 1, i.e., EV, is shifted to the early hours of the planning horizon when the electricity price is minimum. Regarding its operating window, the load type 2, i.e., washing machine, is scheduled in the middle of the day with the shoulder price. The load type 3, i.e., clothes dryer, is scheduled in the peak period, due to its operating window. It is noted that non-thermal loads power consumption is considered in the optimization problem as it might affect the constraints such as (22) and (23).

According to Fig. 7, $T_{low}$ is set to a value far below the room temperature such that the LC of the HVAC system is

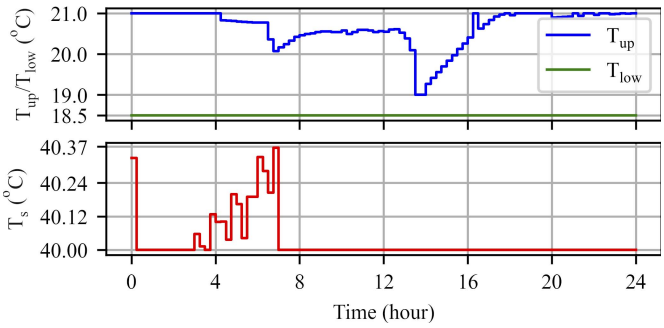


Fig. 7. Optimal set-points of the automatic local controllers.

active in the cooling mode only, as it is expected in summer. The total objective cost is $\hat{O}_N = \$21.72$ from which \$5.1 is the expected energy cost, \$2.13 is the ambiguity cost and the rest is the expected cost of CVaR of constraint violations with a confidence level of $\zeta = 95\%$. It should be noted that the constraint violations exist only in the day-ahead CC optimization problem, while in real time, the thermal constraints (27)-(30) are enforced by the laws of physics. However, effect of the CC optimization problem on constraint violations are projected in the energy cost and/or violation of the zone temperature limits (3)-(4). The computational time for this 24-hour schedule is 9.1 minutes which is compatible for practical use.

For the basic test case in this paper, only one non-thermal controllable load of each type is utilized. In practice, more controllable loads might need to be scheduled, which could affect the computational performance of the proposed method. To comprehensively validate the computational performance, 10 more non-thermal controllable devices (5 interruptible deferrable loads and 5 non-interruptible deferrable loads) are added to the basic test case and the optimization problem is solved again. According to the simulation results, the computational time increases to 12.4 minutes which is still acceptable for the day-ahead scheduling use.

### C. Out-of-Sample Performance Analysis

The out-of-sample performance analysis is an effective tool for measuring solution conservatism of DRO method. It can validate if the ambiguity set is large enough to cover all possible uncertainty PDFs by a reasonable confidence level (as formulated by (50)). As discussed in Section IV-C, the SO-based model can also be achieved through the ambiguity-free case $\epsilon = 0$. Thus, firstly, the problem (43) is solved with a Wasserstein radius $\epsilon = 0.001$. Then, (43) is solved with the day-ahead decisions $\hat{T}_{low}, \hat{T}_{up}, \hat{T}_s$ obtained by DRO, $\epsilon = 0$ and 20 new training samples. Fig. 8 shows the obtained results when this process is repeated for 100 cases. According to Fig. 8, the objective cost of the DRO method is higher for all the cases except two, i.e., iterations 9 and 76. This means the proposed DRO method is robust at a confidence level of 98%.

It is noted that the proper value of Wasserstein ball radius can be selected based on the minimum value of $\epsilon$ that satisfies the required confidence level. Fig. 9 shows the obtained confidence level for different values of the Wasserstein ball

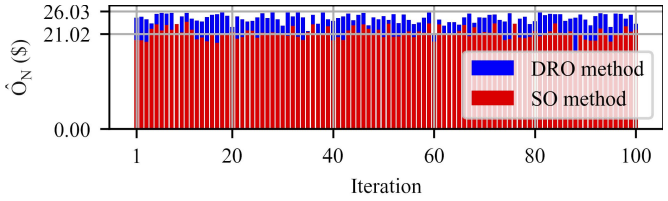


Fig. 8. Out-of-sample performance analysis.

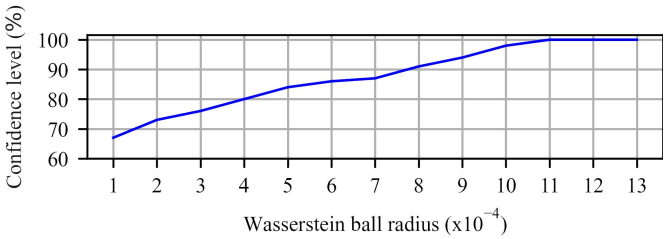


Fig. 9. Solution conservatism with respect to Wasserstein ball radius.

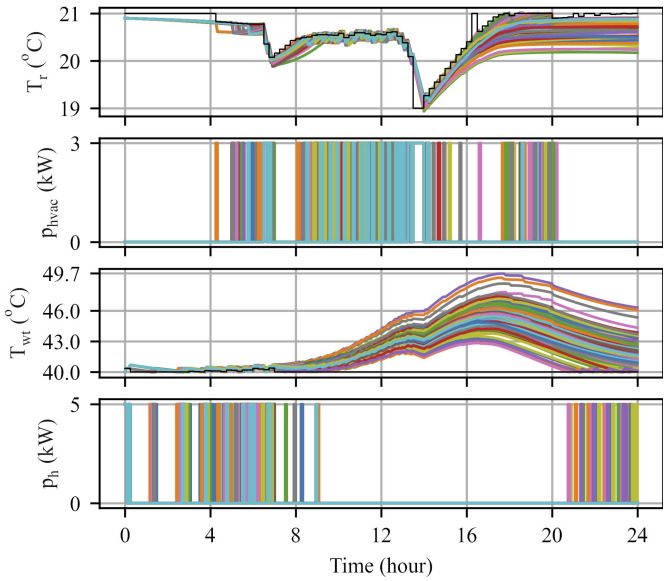


Fig. 10. Local controllers performance - proposed method.

radius $\epsilon$. According to Fig. 9, the conservatism obtaining from the out-of-sample performance analysis could be as poor as 67% for small values of $\epsilon$, while it could be fully conservative for $\epsilon \geq 0.0011$.

### D. Automatic Local Control Performance

As the LC set-points are updated at each DTSC time interval, they respond to real-time variations of their respective thermal zones. In this subsection, using Monte Carlo simulation technique, 100 samples are generated to validate the real-time response of the LCs. Fig. 10 shows power consumption of the HVAC system and the auxiliary heater along with zones temperature for these samples, wherein, the black stepwise curves show the LC set-points. As seen from Fig. 10, the obtained set-points require the LCs to turn on/off HVAC and WH systems in different time points such that the zone temperatures are maintained in the desired ranges. Furthermore,

TABLE III
COMPARISON OF DIFFERENT CONTROL METHODS

| Control method | Energy cost | Temperature deviation | |
|---|---|---|---|
| | | average | maximum |
| Hierarchical coordination | \$5.52 | 0.0000 $^oC$ | 0.0113 $^oC$ |
| Non-coordinated hierarchical | \$6.13 | 0.0002 $^oC$ | 0.0325 $^oC$ |
| Central control | \$6.53 | 0.0301 $^oC$ | 1.3963 $^oC$ |

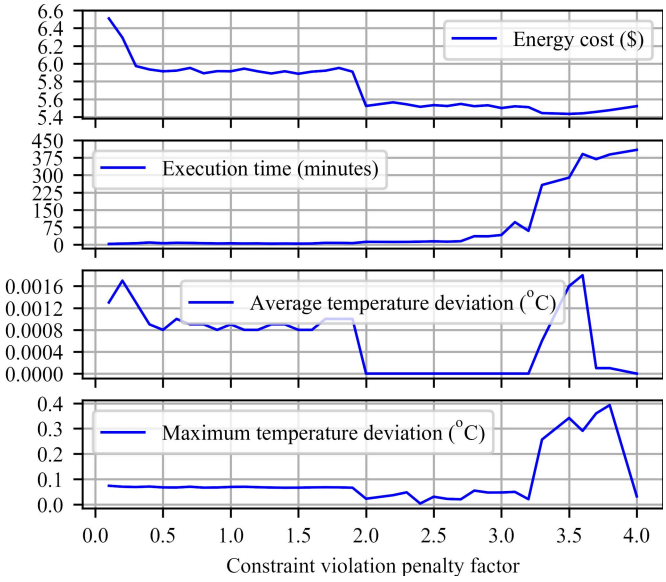


Fig. 11. Sensitivity analysis on the constraint violation penalty factor.

as summarized in Table III, the expected energy cost is \$5.52. Also, average and maximum deviation of zone temperatures from the desired range is negligible.

The constraint violation penalty factor $\rho$ can affect the energy cost, execution time, and zone temperature deviations. Here, sensitivity analysis is implemented to illustrate the effects of the penalty factor $\rho$ on the performance of the proposed model.

According to Fig. 11, small values of $\rho$ leads to high energy cost and large values of $\rho$ results in low energy cost. However, high values of $\rho$ could significantly increase the execution time of the proposed model. Moreover, the average temperature deviations are negligible for all values of $\rho$, while the maximum temperature deviations could be as high as 0.4 $^o$C for large values of $\rho$. From this analysis, it can be concluded that the constraint violation penalty factor $\rho$ should be large enough to preserve the accuracy of the optimization model and also small enough to allow a reasonable execution time. Herein, any value of $2 \leq \rho \leq 3$ can preserve the model accuracy and yet lead to short execution time.

### *E. Comparison With Other Methods*

In this subsection, the proposed hierarchical coordination method is compared to the central control and the non-coordinated hierarchical control methods. For the central control method, the LCs are removed such that HVAC and WH systems follow the day-ahead optimized schedule only. For

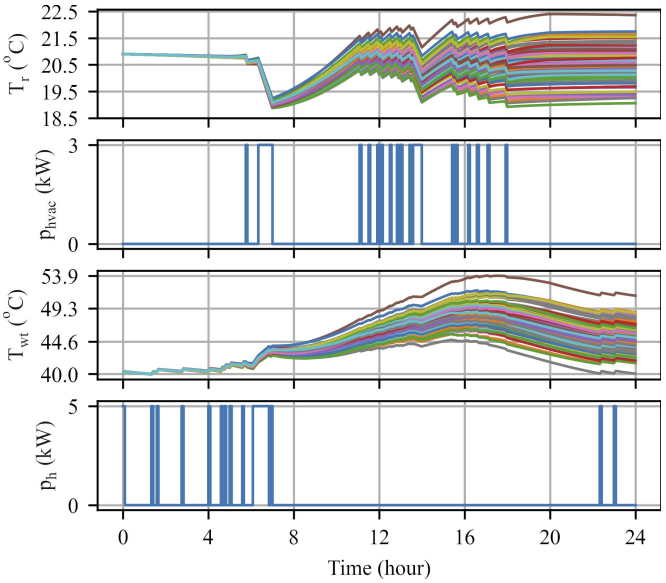


Fig. 12. Central control method results.

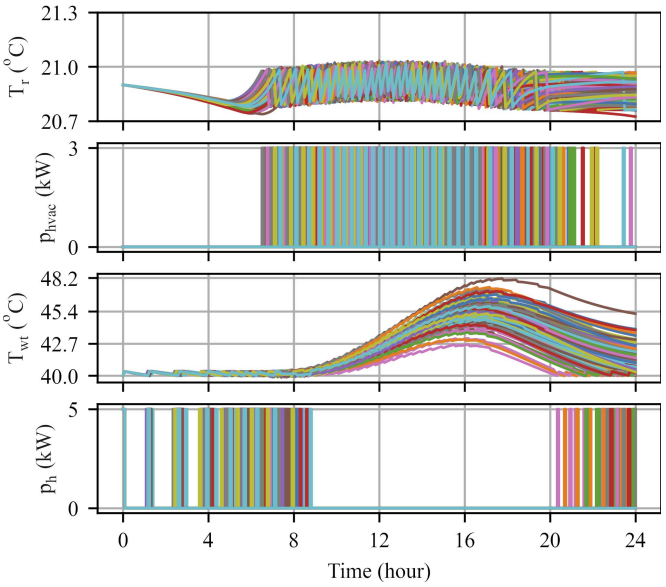


Fig. 13. LCs performance - non-coordinated method.

the non-coordinated hierarchical control method, the proposed DRO method is modified by fixing the LC set-points at arbitrary values $T_{up} = 20.97, T_{low} = 18.5, T_s = 40.02$. The thermal zone thermodynamics along with HVAC and WH schedule for the central control and the non-coordinated hierarchical control methods are illustrated in Fig. 12 and Fig. 13, respectively. In addition, Table III summarizes the obtained results in terms of energy cost and temperature deviation for all the three methods.

According to Fig. 12 and Table III, the central control method cannot maintain the temperatures in the desired ranges for 45 samples where the temperature deviation can be significant as 1.4 $^o$C. Moreover, the central control method leads to highest energy cost in comparison with the others. On the other hand, as seen from Fig. 13 and Table III, the LCs have

satisfying performance in reducing temperature deviations. However, with lack of coordination between central and local control hierarchies, the non-coordinated method increases the expected daily energy cost to \$6.13, i.e., 11% higher than the proposed method. In summary, the proposed hierarchical coordination method leads to least expected energy cost and efficiently maintains the temperatures in the desired ranges.

## VI. Conclusion

In this paper, a data-driven distributionally robust hierarchical coordination control method for HEM is proposed. The proposed method can robustly coordinate the central and the automatic local controllers in a single day-ahead optimization problem using finite historical training dataset.

Via the numerical simulations, it is indicated that, compared to the conventional methods, the proposed hierarchical coordination method can efficiently achieve 11% reduction in the energy cost with the superior out-of-sample performance. Comprehensive analysis indicated that the constraint violation penalty factor must be selected to a value large enough to preserve the model accuracy and yet small enough to maintain the reasonable execution time. Furthermore, extensive sensitivity analysis on different values of the Wasserstein ball radius shows the conservatism of the proposed method can be adjusted to satisfy the desired confidence level requirement.

In future works, the proposed approach can be extended with consideration of battery energy storage systems and power export limits.

## References


[1] (2019). *World Energy Outlook 2019*. [Online]. Available: https://www.iea.org/reports/world-energy-outlook-2019

[2] A. Anvari-Moghaddam, A. Rahimi-Kian, M. S. Mirian, and J. M. Guerrero, "A multi-agent based energy management solution for integrated buildings and microgrid system," *Appl. Energy*, vol. 203, pp. 41–56, Oct. 2017.

[3] Y. Liu *et al.*, "Coordinating the operations of smart buildings in smart grids," *Appl. Energy*, vol. 228, pp. 2510–2525, Oct. 2018.

[4] Z. Xu, X. Guan, Q.-S. Jia, J. Wu, D. Wang, and S. Chen, "Performance analysis and comparison on energy storage devices for smart building energy management," *IEEE Trans. Smart Grid*, vol. 3, no. 4, pp. 2136–2147, Dec. 2012.

[5] M. Ortiz, H. Barsun, H. He, P. Vorobieff, and A. Mammoli, "Modeling of a solar-assisted HVAC system with thermal storage," *Energy Build.*, vol. 42, no. 4, pp. 500–509, 2010.

[6] H. T. Nguyen, D. T. Nguyen, and L. B. Le, "Energy management for households with solar assisted thermal load considering renewable energy and price uncertainty," *IEEE Trans. Smart Grid*, vol. 6, no. 1, pp. 301–314, Jan. 2015.

[7] L. Pérez-Lombard, J. Ortiz, and C. Pout, "A review on buildings energy consumption information," *Energy Build.*, vol. 40, no. 3, pp. 394–398, 2008.

[8] B. Sun, P. B. Luh, Q.-S. Jia, Z. Jiang, F. Wang, and C. Song, "Building energy management: Integrated control of active and passive heating, cooling, lighting, shading, and ventilation systems," *IEEE Trans. Autom. Sci. Eng.*, vol. 10, no. 3, pp. 588–602, Jul. 2013.

[9] A. Baniasadi, D. Habibi, O. Bass, and M. A. S. Masoum, "Optimal real-time residential thermal energy management for peak-load shifting with experimental verification," *IEEE Trans. Smart Grid*, vol. 10, no. 5, pp. 5587–5599, Sep. 2019.

[10] J. Aguilar, A. Garcès-Jimènez, N. Gallego-Salvador, J. A. G. De Mesa, J. M. Gomez-Pulido, and J. García-Tejedor, "Autonomic management architecture for multi-HVAC systems in smart buildings," *IEEE Access*, vol. 7, pp. 123402–123415, 2019.

[11] A. Anvari-Moghaddam, H. Monsef, and A. Rahimi-Kian, "Optimal smart home energy management considering energy saving and a comfortable lifestyle," *IEEE Trans. Smart Grid*, vol. 6, no. 1, pp. 324–332, Jan. 2015.

[12] E. Ahmadi, Y. Noorollahi, B. Mohammadi-Ivatloo, and A. Anvari-Moghaddam, "Stochastic operation of a solar-powered smart home: Capturing thermal load uncertainties," *Sustainability*, vol. 12, no. 12, p. 5089, Jun. 2020.

[13] A. Anvari-Moghaddam, J. M. Guerrero, J. C. Vasquez, H. Monsef, and A. Rahimi-Kian, "Efficient energy management for a grid-tied residential microgrid," *IET Gener. Transm. Distrib.*, vol. 11, no. 11, pp. 2752–2761, Aug. 2017.

[14] F. Luo, W. Kong, G. Ranzi, and Z. Y. Dong, "Optimal home energy management system with demand charge tariff and appliance operational dependencies," *IEEE Trans. Smart Grid*, vol. 11, no. 1, pp. 4–14, Jan. 2020.

[15] X. Hou, J. Wang, T. Huang, T. Wang, and P. Wang, "Smart home energy management optimization method considering energy storage and electric vehicle," *IEEE Access*, vol. 7, pp. 144010–144020, 2019.

[16] M. Nistor and C. H. Antunes, "Integrated management of energy resources in residential buildings—A Markovian approach," *IEEE Trans. Smart Grid*, vol. 9, no. 1, pp. 240–251, Jan. 2018.

[17] F. Wei *et al.*, "A novel thermal energy storage system in smart building based on phase change material," *IEEE Trans. Smart Grid*, vol. 10, no. 3, pp. 2846–2857, May 2019.

[18] V. Pilloni, A. Floris, A. Meloni, and L. Atzori, "Smart home energy management including renewable sources: A QoE-driven approach," *IEEE Trans. Smart Grid*, vol. 9, no. 3, pp. 2006–2018, May 2018.

[19] D. T. Vedullapalli, R. Hadidi, and B. Schroeder, "Combined HVAC and battery scheduling for demand response in a building," *IEEE Trans. Ind. Appl.*, vol. 55, no. 6, pp. 7008–7014, Nov./Dec. 2019.

[20] S. Althaher, P. Mancarella, and J. Mutale, "Automated demand response from home energy management system under dynamic pricing and power and comfort constraints," *IEEE Trans. Smart Grid*, vol. 6, no. 4, pp. 1874–1883, Jul. 2015.

[21] C. Zhang, Y. Xu, Z. Li, and Z. Y. Dong, "Robustly coordinated operation of a multi-energy microgrid with flexible electric and thermal loads," *IEEE Trans. Smart Grid*, vol. 10, no. 3, pp. 2765–2775, May 2019.

[22] X. Qin, S. Lysecky, and J. Sprinkle, "A data-driven linear approximation of HVAC utilization for predictive control and optimization," *IEEE Trans. Control Syst. Technol.*, vol. 23, no. 2, pp. 778–786, Mar. 2015.

[23] E. Delage and Y. Ye, "Distributionally robust optimization under moment uncertainty with application to data-driven problems," *Oper. Res.*, vol. 58, no. 3, pp. 595–612, 2010.

[24] R. Jiang and Y. Guan, "Data-driven chance constrained stochastic program," *Math. Program.*, vol. 158, pp. 291–327, Jul. 2016.

[25] P. M. Esfahani and D. Kuhn, "Data-driven distributionally robust optimization using the Wasserstein metric: Performance guarantees and tractable reformulations," *Math. Program.*, vol. 171, pp. 115–166, Jul. 2017.

[26] P. Zhao, H. Wu, C. Gu, and I. Hernando-Gil, "Optimal home energy management under hybrid photovoltaic-storage uncertainty: A distributionally robust chance-constrained approach," *IET Renew. Power Gener.*, vol. 13, no. 11, pp. 1911–1919, 2019.

[27] Y. F. Du, L. Jiang, C. Duan, Y. Z. Li, and J. S. Smith, "Energy consumption scheduling of HVAC considering weather forecast error through the distributionally robust approach," *IEEE Trans. Ind. Informat.*, vol. 14, no. 3, pp. 846–857, Mar. 2018.

[28] Z. Wang, P. W. Glynn, and Y. Ye, "Likelihood robust optimization for data-driven problems," *Comput. Manage. Sci.*, vol. 13, no. 2, pp. 241–261, Sep. 2015.

[29] J. Goh and M. Sim, "Distributionally robust optimization and its tractable approximations," *Oper. Res.*, vol. 58, pp. 902–917, Aug. 2010.

[30] Y. Guo, K. Baker, E. Dall'Anese, Z. Hu, and T. H. Summers, "Data-based distributionally robust stochastic optimal power flow—Part I: Methodologies," *IEEE Trans. Power Syst.*, vol. 34, no. 2, pp. 1483–1492, Mar. 2019.

[31] R. Zhu, H. Wei, and X. Bai, "Wasserstein metric based distributionally robust approximate framework for unit commitment," *IEEE Trans. Power Syst.*, vol. 34, no. 4, pp. 2991–3001, Jul. 2019.

[32] C. Zhang, Z. Y. Dong, and X. Yin, "Affinely adjustable robust energy management system for smart homes," *IET Renew. Power Gener.*, vol. 14, no. 15, pp. 2955–2965, Nov. 2020.
[33] R. T. Rockafellar and S. Uryasev, "Optimization of conditional value-at-risk," *J. Risk*, vol. 2, no. 3, pp. 21–41, 2000.
[34] *An Easy Way to Find, Explore and Reuse Australia's Public Data*. Accessed: Sep. 2020. [Online]. Available: https://data.gov.au/
[35] *AGL Internet is Here*. Accessed: Sep. 2020. [Online]. Available: https://www.agl.com.au/
[36] Gurobi Optimization LLC. (2021). *Gurobi Optimizer Reference Manual*. [Online]. Available: http://www.gurobi.com

**Hossein Saberi** received the B.Sc. degree in electrical engineering from Shahid Rajaee Teacher Training University, Iran, in 2013, and the M.Sc. degree in power systems and high voltage engineering from the University of Tehran, Iran, in 2015. He is currently pursuing the Ph.D. degree in electrical engineering with the University of New South Wales, Australia. His research interests include power system planning, operation, protection, transient stability, frequency stability, demand-side management, and applications of mathematical optimization theories and machine learning techniques.

**Cuo Zhang** (Member, IEEE) received the B.E. degree (Hons.) in electrical (power) engineering from the University of Sydney, Australia, in 2014, and the Ph.D. degree in electrical engineering from the University of New South Wales, Australia, in 2018, where he is currently a Research Fellow. His research interests include power system planning and operation, voltage stability and control, demand side management, microgrids, multienergy systems, and applications of optimization theory and artificial intelligence in these areas. He was a recipient of the two IEEE PES General Meeting Best Conference Papers, IEEE TRANSACTIONS ON SMART GRID Best Reviewer, the UNSW Promoting High Quality Research Papers Scheme Award, and the University Medal from the University of Sydney.

**Zhao Yang Dong** (Fellow, IEEE) received the Ph.D. degree from the University of Sydney, Australia, in 1999. He is currently a SHARP Professor and the Director of the UNSW Digital Grid Futures Institute, University of New South Wales, Australia. He was a Ausgrid Chair and the Director of the Ausgrid Centre for Intelligent Electricity Networks providing support for the smart grid, smart city national demonstration project. His research interests include smart grid, power system planning and stability, renewable energy systems, electricity market, and computational methods for power engineering applications. He has served/is serving as an editor for a number of IEEE transactions and IET journals. He is a Web of Science Highly Cited Researcher.